

Alma Mater Studiorum Università di Bologna  
Archivio istituzionale della ricerca

Buoyancy-Induced Instability of a Power-Law Fluid Saturating a Vertical Porous Slab

This is the final peer-reviewed author's accepted manuscript (postprint) of the following publication:

*Published Version:*

Lazzari S., Celli M., Vayssiere Brandão P., Barletta A. (2023). Buoyancy-Induced Instability of a Power-Law Fluid Saturating a Vertical Porous Slab. ASME JOURNAL OF HEAT AND MASS TRANSFER, 145(4), 1-8 [10.1115/1.4055859].

*Availability:*

This version is available at: <https://hdl.handle.net/11585/941367> since: 2023-09-12

*Published:*

DOI: <http://doi.org/10.1115/1.4055859>

*Terms of use:*

Some rights reserved. The terms and conditions for the reuse of this version of the manuscript are specified in the publishing policy. For all terms of use and more information see the publisher's website.

This item was downloaded from IRIS Università di Bologna (<https://cris.unibo.it/>).  
When citing, please refer to the published version.

(Article begins on next page)

This is the final peer-reviewed accepted manuscript of:

**Lazzari, S., Celli, M., Vayssière Brandão, P., and Barletta, A. (December 19, 2022). "Buoyancy-Induced Instability of a Power-Law Fluid Saturating a Vertical Porous Slab." ASME. *J. Heat Mass Transfer*. April 2023; 145(4): 042601**

The final published version is available online at:

<https://doi.org/10.1115/1.4055859>

#### Terms of use:

Some rights reserved. The terms and conditions for the reuse of this version of the manuscript are specified in the publishing policy. For all terms of use and more information see the publisher's website.

*This item was downloaded from IRIS Università di Bologna (<https://cris.unibo.it/>)*

***When citing, please refer to the published version.***

# Buoyancy-induced instability of a power-law fluid saturating a vertical porous slab

**Stefano Lazzari**  
Professor

Dept. Architecture and Design  
Polytechnic School, University of Genoa  
Stradone S. Agostino 37, 16123, Genoa  
Email: stefano.lazzari@unige.it

**Michele Celli**  
Professor

Dept. Industrial Engineering  
Alma Mater Studiorum Università di Bologna  
Via Risorgimento 2, 40136, Bologna, Italy  
Email: michele.celli3@unibo.it

**Pedro Vayssi re Brand o**  
Research Fellow

Dept. Industrial Engineering  
Alma Mater Studiorum Università di Bologna  
Via Risorgimento 2, 40136, Bologna, Italy  
Email: pedro.vayssiere2@unibo.it

**Antonio Barletta\***  
Full Professor

Dept. Industrial Engineering  
Alma Mater Studiorum Università di Bologna  
Via Risorgimento 2, 40136, Bologna, Italy  
Email: antonio.barletta@unibo.it

*Many engineering applications involve porous media and rely on non-Newtonian working fluids. In the present paper, the seepage flow of a non-Newtonian fluid saturating a vertical porous layer is studied. The buoyant flow is thermally driven by the boundaries of the porous layer, which are permeable surfaces kept at different temperatures. In order to model the seepage flow of both shear-thinning (pseudoplastic) and shear-thickening (dilatant) fluids, reference is made to the Ostwald-de Waele rheological model implemented with the power-law extended form of Darcy's law.*

*The basic stationary flow is parallel to the vertical axis and shows a single-cell pattern, where the cell has infinite height and can display a core-region of enhanced/inhibited flow according to the fluid's rheological behaviour. By applying small perturbations, a linear stability analysis of the basic flow is performed to determine the onset conditions for a multicellular pattern. This analysis is carried out numerically by employing the shooting method. The neutral stability curves and the values of the critical Rayleigh number are computed for different pseudoplastic and dilatant fluids. The behaviour of a Newtonian fluid is also obtained as a limiting case.*

---

\* Address all correspondence to this author.

## NOMENCLATURE

### Latin symbols

$c$	Specific heat
$\mathbf{e}_y$	Unit vector in the $y$ -direction
$f$	Eigenfunction
$F$	Real function
$g$	Modulus of gravitational acceleration
$\mathbf{g}$	Gravity vector
$h$	Eigenfunction
$k$	Thermal conductivity
$K$	Permeability of the porous layer
$L$	Layer thickness
$n$	Power-law fluid index
$p$	Local difference between the pressure and the hydrostatic pressure
$P$	Pressure perturbation
$R$	Modified Darcy-Rayleigh number
$t$	Time
$T$	Temperature
$T_0$	Reference temperature
$T_1$	Temperature of the external reservoir in $x \leq -L/2$
$T_2$	Temperature of the external reservoir in $x \geq L/2$
$\mathbf{u}$	Velocity vector, $(u, v, w)$
$\mathbf{U}$	Velocity perturbation

$\mathbf{x}$  Position vector,  $(x, y, z)$

*Greek symbols*

$\alpha$  Wave number  
 $\beta$  Fluid thermal expansion coefficient  
 $\delta$  Smoothing parameter  
 $\Delta T$  Temperature gap between the boundaries  
 $\varepsilon$  Dimensionless perturbation parameter  
 $\eta$  Consistency factor  
 $\Theta$  Temperature perturbation  
 $\lambda$  Growth rate  
 $\mu$  Dynamic viscosity  
 $\xi_1, \xi_2$  Real parameters  
 $\rho$  Density  
 $\sigma$  Heat capacity ratio  
 $\varphi$  Porosity  
 $\phi$  Inclination angle  
 $\chi$  Effective thermal diffusivity  
 $\omega$  Angular frequency

*Subscripts*

$b$  Basic state  
 $c$  Critical value  
 $eff$  Effective (saturated porous medium)  
 $f$  Fluid  
 $s$  Solid

## 1 INTRODUCTION

It is widely known that the non-Newtonian rheology of working fluids is of uttermost importance in many engineering applications. The development of new ideas for the design of heat transfer enhancement systems or thermal energy storage devices often involve the analysis of fluid saturated porous media. For instance, the use of highly-conductive porous materials such as the metallic foams turns out to improve the overall thermal conductance in compact heat exchangers. The use of liquids with a non-Newtonian behaviour can be important when a thermal energy storage effect is sought or when the heat transfer enhancement is pursued via nanofluids. Beyond such applications relative to mechanical and thermal engineering, there is an interest for the non-Newtonian flows in porous media in the chemical engineering area when polymeric liquid processing or filtration is considered.

The apparent viscosity of a fluid, namely the ratio between shear stress and shear rate, can be time-independent or time-dependent. The first class of fluids include not only Newtonian fluids and Bingham plastics, but also shear-thinning fluids (often referred to as pseudoplastic) and shear-thickening (or dilatant) fluids. Newtonian fluids and Bingham plastics display a constant viscosity and possibly a threshold finite yield stress. On the

other hand, the viscosity of pseudoplastic and dilatant fluids decreases or increases as shear stress increases [1], respectively. Moreover, there are fluids that exhibit a behaviour similar to the cited fluids with respect to shear stress and whose viscosity depends also on time, such as thixotropic and rheopectic fluids, where the shear stress decreases or increases, respectively, with increasing time of application of a constant shear rate [2].

The power-law rheology, also termed Ostwald-de Waele, models both time-independent shear-thinning and shear-thickening fluids through an index  $n$ . Indeed, for  $n < 1$  and  $n > 1$ , the pseudoplastic and dilatant behaviours are retrieved, respectively, whereas the limiting case  $n = 1$  models the Newtonian fluid. Power-law fluids are adopted in a wide variety of applications, in chemical and food industries, in geophysics (drilling fluids and cements that are used for geothermal and petroleum well construction), in buildings construction (for instance, clay suspensions, plaster and concrete mix, usage of surfactants in district and building heating and cooling systems to allow energy savings [3]). We also mention pharmaceuticals industry, automotive traction control and innovative body armors, when mixed with Kevlar®. Thus, there exists a wide scientific literature about heat and mass transfer problems for such fluids [4–8].

When it comes to the stability analysis of the buoyant flow in a vertical porous layer saturated by a non-Newtonian fluid, the number of available papers is still quite low. Starting from the pioneering work by Gill [9], proofs exist that natural convection of a Newtonian fluid in a vertical porous slab with impermeable walls kept at different but uniform temperatures is always stable, in the so-called conduction regime [10–14]. Later, Barletta and Alves [15] extended this classical stability problem by considering a power-law fluid and concluded that all longitudinal rolls are stable and present smaller damping rates than oblique and transverse rolls. Moreover, they proved numerically that the transition to convective instability cannot be achieved even for high values of the Darcy-Rayleigh number. Recently, the convective instability for the vertical buoyant flow of a viscoelastic Oldroyd-B fluid saturating a vertical porous layer was investigated [16, 17]. In particular, Lazzari et al. [17] carried out the stability analysis by assuming open boundaries and pointing out the destabilising effect of viscoelasticity. We also mention the recent studies involving the thermal instability and convection in Bingham-fluid saturated porous media [18–20].

In the present paper, a problem similar to that discussed in [15], but with different boundary conditions is considered. Namely, the linear stability of natural convection of a power-law fluid saturating a vertical porous slab

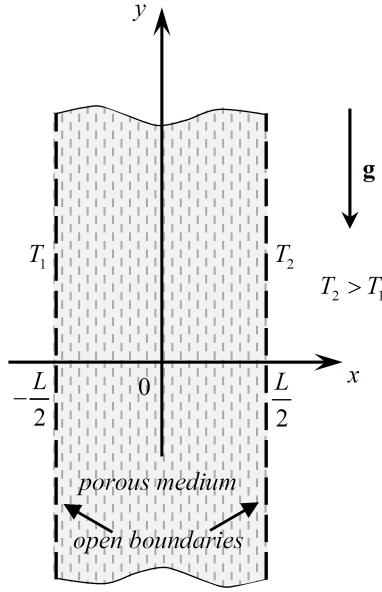


Fig. 1. Cross-section of the vertical porous slab in the  $xy$ -plane with the adopted boundary conditions

which is confined by two isothermal yet permeable surfaces, *i.e.*, by two open boundaries kept at different temperatures. The Newtonian version of this problem was investigated by Barletta [21]. The forthcoming analysis is carried out numerically in order to find the neutral stability curves for different pseudoplastic and dilatant fluids and to obtain the critical values of the modified Darcy–Rayleigh number that determine the flow instability. The particular case of a Newtonian fluid is also treated as a limiting case for benchmarking purposes.

## 2 MATHEMATICAL MODEL

A homogeneous isotropic vertical porous layer saturated by a non-Newtonian fluid is considered. While the layer has thickness  $L$  in the horizontal  $x$ -direction, it is infinitely wide in the vertical  $y$ -direction as well as in the spanwise  $z$ -direction. A sketch of the layer is shown in Fig. 1.

The Ostwald–de Waele power-law model, where the nonlinear relationship between stress and shear rate is parametrised by an index  $n$ , is adopted to describe the non-Newtonian rheology of the fluid. Darcy’s law for Ostwald–de Waele type of fluid is written as [4]

$$\frac{\eta |\mathbf{u}|^{n-1}}{K} \mathbf{u} = -\nabla p, \quad (1)$$

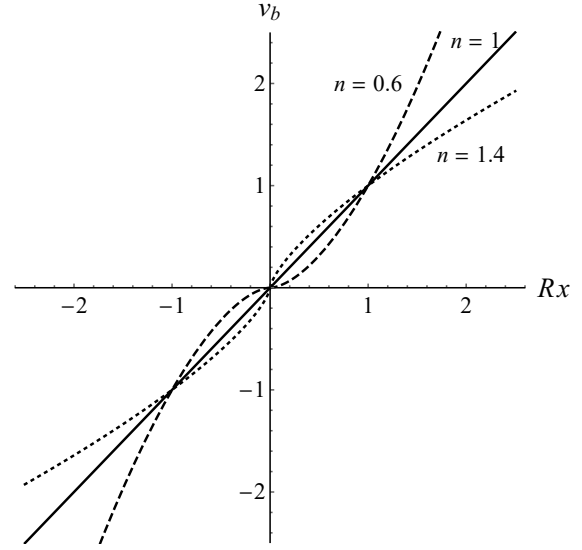


Fig. 2. Basic velocity profile for a pseudoplastic fluid ( $n = 0.6$ ), for a Newtonian fluid ( $n = 1$ ) and for a dilatant fluid ( $n = 1.4$ )

where  $K [m^{n+1}]$  is the generalized permeability and  $\eta [Pa s^n]$  is the consistency factor. As can be inferred from Eqn. (1), the Newtonian case  $n = 1$  yields the classical Darcy’s law, while  $n < 1$  and  $n > 1$  describe pseudoplastic and dilatant behaviours, respectively.

The buoyancy force is modelled by means of the Oberbeck–Boussinesq approximation and the local energy balance equation, where no source or sink term is considered and viscous dissipation is neglected, is employed to model the heat transfer.

The vertical boundaries of the slab are permeable and the external environments in the regions  $x < -L/2$  and  $x > L/2$  are considered as isothermal fluid reservoirs in a motionless state, so that the pressure distribution along the boundaries is purely hydrostatic. Since the external fluid reservoirs are kept at different uniform temperatures  $T_1$  and  $T_2$ , where  $T_2 > T_1$ , the layer is subject to side heating, as depicted in Fig. 1.

Accordingly, the governing balance equations for mass, momentum and energy as well as the adopted boundary conditions are given by

$$\nabla \cdot \mathbf{u} = 0, \quad (2)$$

$$\frac{\eta |\mathbf{u}|^{n-1}}{K} \mathbf{u} = -\nabla p + \rho_f g \beta (T - T_0) \mathbf{e}_y, \quad (3)$$

$$\sigma \frac{\partial T}{\partial t} + \mathbf{u} \cdot \nabla T = \chi \nabla^2 T, \quad (4)$$

$$\begin{aligned} x = -L/2 : \quad p &= 0, \quad T = T_1, \\ x = +L/2 : \quad p &= 0, \quad T = T_2, \end{aligned} \quad (5)$$

where  $g$  and  $\mathbf{e}_y$  are the modulus of  $\mathbf{g}$  and the unit vector along the  $y$ -direction, respectively. In Eqn. (3), the fluid density  $\rho_f$  is evaluated at the reference temperature  $T_0 = (T_1 + T_2)/2$ , and the parameters  $\sigma$ ,  $k_{eff}$  and  $\chi$  are defined as

$$\begin{aligned} \sigma &= \frac{\varphi \rho_f c_f + (1 - \varphi) \rho_s c_s}{\rho_f c_f}, \\ k_{eff} &= \varphi k_f + (1 - \varphi) k_s, \quad \chi = \frac{k_{eff}}{\rho_f c_f}. \end{aligned} \quad (6)$$

The dimensionless formulation of the problem is obtained by means of the following scaling:

$$\begin{aligned} \frac{\mathbf{x}}{L} &\rightarrow \mathbf{x}, \quad \frac{\chi}{\sigma L^2} t \rightarrow t, \quad \frac{K L^{n-1}}{\eta \chi^n} p \rightarrow p, \\ \frac{L}{\chi} \mathbf{u} &\rightarrow \mathbf{u}, \quad \frac{T - T_0}{\Delta T} \rightarrow T, \\ L \nabla &\rightarrow \nabla, \quad L^2 \nabla^2 \rightarrow \nabla^2, \end{aligned} \quad (7)$$

where  $\Delta T = T_2 - T_1$ . By substituting Eqn. (7) in Eqns. (2)–(5), the following dimensionless governing equations are obtained

$$\nabla \cdot \mathbf{u} = 0, \quad (8)$$

$$|\mathbf{u}|^{n-1} \mathbf{u} = -\nabla p + R T \mathbf{e}_y, \quad (9)$$

$$\frac{\partial T}{\partial t} + \mathbf{u} \cdot \nabla T = \nabla^2 T, \quad (10)$$

$$\begin{aligned} x = -1/2 : \quad p &= 0, \quad T = -1/2, \\ x = +1/2 : \quad p &= 0, \quad T = +1/2, \end{aligned} \quad (11)$$

where the modified Darcy–Rayleigh number  $R$  is

$$R = \frac{\rho_f g \beta \Delta T K L^n}{\eta \chi^n}. \quad (12)$$

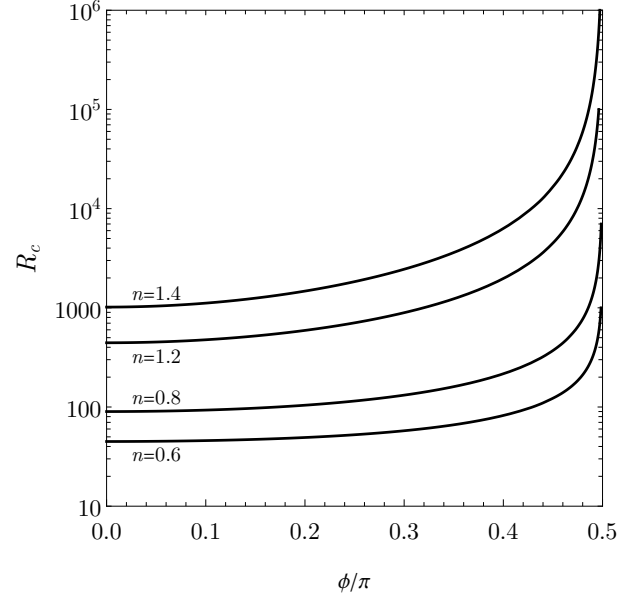


Fig. 3. Trend of  $R_c$  versus  $\phi$  for different values of  $n$

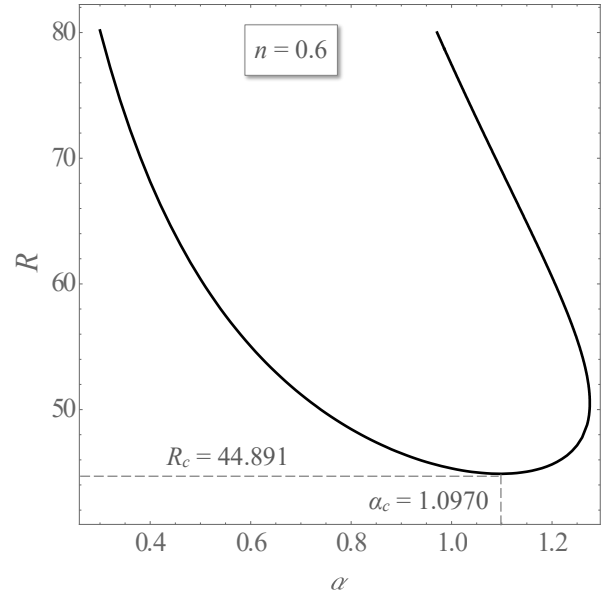


Fig. 4. Neutral stability curve for a pseudoplastic fluid with  $n = 0.6$  and critical values of  $R$  and  $\alpha$

### 3 LINEAR STABILITY ANALYSIS

#### 3.1 Basic state

The problem described by Eqns. (8)–(11) features a stationary fully developed buoyant flow solution where the flow is bidirectional with a vanishing net mass flow rate. The only non-vanishing component of the seepage velocity is  $v_b$ , along the  $y$ -direction. The basic stationary

solution of Eqns. (8)–(11) is given by

$$\mathbf{u}_b = (0, Rx F(x), 0), \quad p_b = 0, \quad T_b = x, \quad (13)$$

where  $F(x) = (R^2 x^2)^{\frac{1-n}{2n}}$ ,

which describes a single-cell vertical pattern where the cell has an infinite height. Figure 2 shows the basic velocity profile  $v_b$  as a function of  $Rx$  for a pseudoplastic fluid ( $n = 0.6$ ), for a Newtonian fluid ( $n = 1$ ) and for a dilatant fluid ( $n = 1.4$ ). In the first case (dashed line), the flow is inhibited in the core region around the midplane  $x = 0$ , while it is enhanced in the same region for the last case (dotted line). Details about this behaviour can be found in [9],[15].

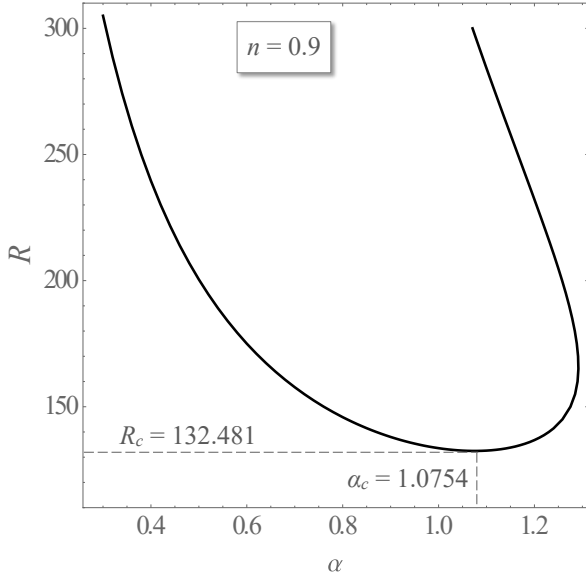


Fig. 5. Neutral stability curve for a pseudoplastic fluid with  $n = 0.9$  and critical values of  $R$  and  $\alpha$

### 3.2 Eigenvalue problem for neutrally stable modes

The linear stability analysis of the basic flow starts by perturbing it through small-amplitude disturbances,

$$\begin{aligned} \mathbf{u} &= \mathbf{u}_b + \varepsilon \mathbf{U}, \\ p &= p_b + \varepsilon P, \\ T &= T_b + \varepsilon \Theta, \end{aligned} \quad (14)$$

where  $\varepsilon \ll 1$ . By substituting Eqn. (14) into Eqns. (8)–(11), by neglecting  $O(\varepsilon^2)$  terms and by rearranging

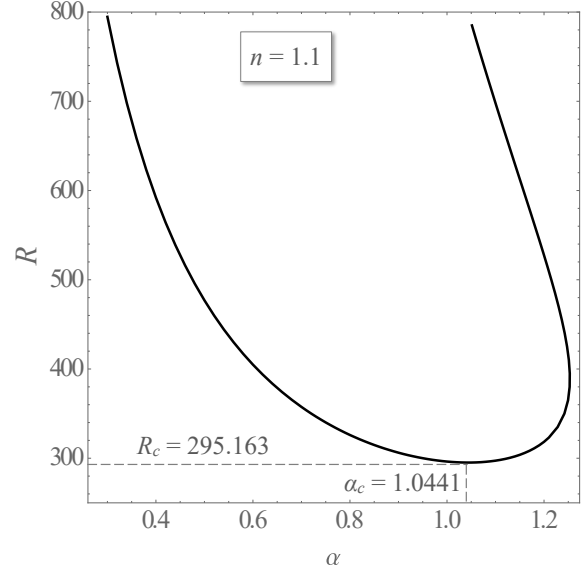


Fig. 6. Neutral stability curve for a dilatant fluid with  $n = 1.1$  and critical values of  $R$  and  $\alpha$

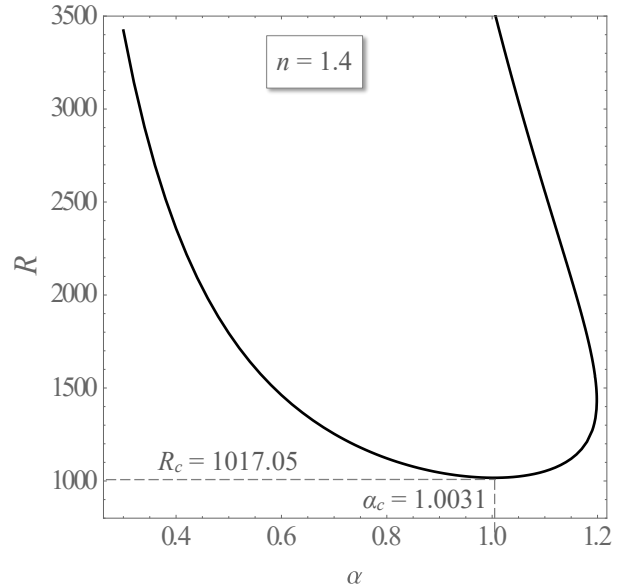


Fig. 7. Neutral stability curve for a dilatant fluid with  $n = 1.4$  and critical values of  $R$  and  $\alpha$

the equations to obtain a more convenient pressure–temperature formulation, we obtain

$$-F'(x) \frac{\partial P}{\partial x} + \frac{1}{n} F(x) \left[ R \frac{\partial \Theta}{\partial y} - \frac{\partial^2 P}{\partial y^2} - n \left( \frac{\partial^2 P}{\partial x^2} + \frac{\partial^2 P}{\partial z^2} \right) \right] = 0, \quad (15)$$

$$\frac{\partial \Theta}{\partial t} - F(x) \frac{\partial P}{\partial x} + R x F(x) \frac{\partial \Theta}{\partial y} - \nabla^2 \Theta = 0, \quad (16)$$

$$x = \pm 1/2: \quad P = 0, \quad \Theta = 0. \quad (17)$$

The pressure and temperature perturbations are assumed to have the form of normal modes, namely

$$P(x, y, t) = i f(x) e^{(\lambda - i \omega) t} e^{i(\alpha \cos \phi y + \alpha \sin \phi z)}, \quad (18)$$

$$\Theta(x, y, t) = h(x) e^{(\lambda - i \omega) t} e^{i(\alpha \cos \phi y + \alpha \sin \phi z)}, \quad (19)$$

where the parameters  $(\alpha, \phi, \lambda, \omega)$  are real, while  $(f, h)$  are, in general, complex functions. The angle  $\phi$  defines general oblique rolls. The special cases  $\phi = 0$  and  $\phi = \pi/2$  describe transverse rolls and longitudinal rolls, respectively. The growth rate  $\lambda$  marks the difference between stability ( $\lambda < 0$ ) and instability ( $\lambda > 0$ ). The neutrally stable configuration is identified by  $\lambda = 0$ . In this case, the condition of minimum  $R$  among the neutrally stable modes defines the critical values  $\alpha_c$  and  $R_c$  for the onset of convective rolls.

By substituting Eqns. (18) and (19) into Eqns. (15)–(17), the following eigenvalue problem for neutrally stable modes is obtained:

$$R \alpha \cos \phi F(x) h - n [f' F'(x) + F(x) f''] + \alpha^2 f F(x) (\cos^2 \phi + n \sin^2 \phi) = 0, \quad (20)$$

$$h'' + i f' F(x) - [\alpha^2 + \lambda - i \omega + i \alpha \cos \phi R x F(x)] h = 0, \quad (21)$$

$$x = \pm 1/2: \quad f = 0, \quad h = 0. \quad (22)$$

The solution of the ODEs given by Eqns. (20) and (21) can be found numerically by means of the shooting method. The associated initial value problem is solved with the Runge–Kutta method, while Brent's method is adopted for the root searching procedure. The numerical solution of the problem is here found through the built-in functions `NDSolve` and `FindRoot` available within the Mathematica 12.0 environment (© Wolfram Research). Accordingly, the problem is rewritten as an initial value problem starting from  $x = -1/2$ , namely Eqn. (22) yields

$$f(-1/2) = 0, \quad f'(-1/2) = \xi_1 + i \xi_2, \quad (23)$$

$$h(-1/2) = 0, \quad h'(-1/2) = 1, \quad (24)$$

where  $\xi_1$  and  $\xi_2$  are unknown real parameters to be determined by the shooting method, while the last condition on  $h'$  is a scale-fixing condition set to break the scale invariance of the eigenfunctions  $(f, h)$ . According to the method, for given values of the 3 parameters  $(n, \alpha, R)$  one may determine iteratively the values of  $(\lambda, \omega, \xi_1, \xi_2)$  that satisfy the target conditions in  $x = 1/2$ , namely  $f(1/2) = 0$ ,  $h(1/2) = 0$ . However, since the function  $F(x)$  defined by Eqn. (13) has a singularity in  $x = 0$  for  $n \neq 1$ , it is useful to introduce a small positive smoothing parameter  $\delta$  as a workaround against numerical issues by redefining  $F(x)$  as follows

$$F(x) = (R^2 x^2 + \delta)^{\frac{1-n}{2n}}. \quad (25)$$

In the following, the sensitivity of the results to the adopted value of  $\delta$  is checked, for each considered value of  $n$ . The main requirement for an efficient solution of Eqns. (20)–(24) through the shooting method is an accurate initial guess for the eigenvalue quantities  $R$  and  $\omega$ , for a given prescribed input dataset.

#### 4 DISCUSSION OF RESULTS

The change of the inclination angle  $\phi$  accounts for the transition from transverse rolls,  $\phi = 0$ , to longitudinal rolls,  $\phi = \pi/2$ . Figure 3 shows the dependence of the critical Darcy–Rayleigh number on  $\phi$ . This figure allows one to conclude, with reference to the sample cases  $n = 0.6, 0.8, 1.2, 1.4$ , that  $\phi = 0$  yields the least possible value of  $R_c$ . As a consequence, we can consider the transverse rolls as the most unstable perturbations. Thus, in the following, we will focus our analysis only on transverse rolls.

In order to investigate the onset of instability for a wide class of power-law fluids, the behaviour of four pseudoplastic fluids, having  $n = 0.6, 0.7, 0.8, 0.9$ , and four dilatant fluids, having  $n = 1.1, 1.2, 1.3, 1.4$ , is analysed. Moreover, the reference case of a Newtonian fluid ( $n = 1$ ) is also studied. In this case, the basic velocity profile given by Eqn. (13) simplifies to  $v_b = R x$  and, thus, the study does not require the introduction of the smoothing parameter  $\delta$ . The critical values obtained for the case of a Newtonian fluid are  $R_c = 197.081$ ,  $\alpha_c = 1.0595$ , which coincide with what reported in [15]. Figures 4 and 5 show the neutral stability curve for two pseudoplastic fluids, having  $n = 0.6$  and  $n = 0.9$ , respectively. As can be inferred by the comparison, the pseudoplastic fluid

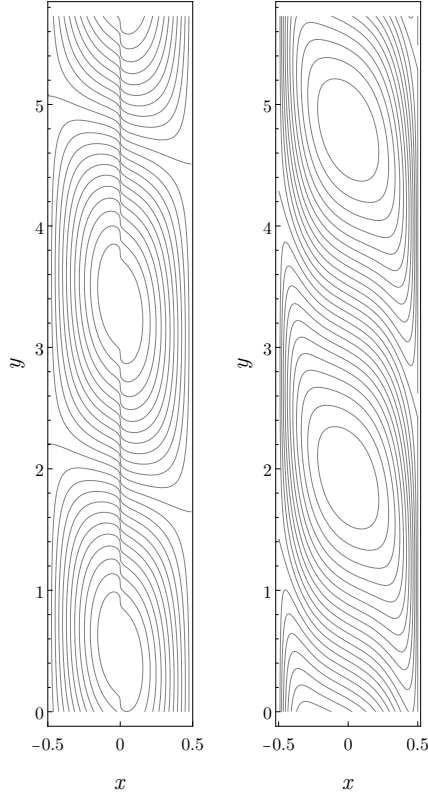


Fig. 8. Dimensionless pressure (left) and temperature (right) contour plot for the perturbations in a pseudoplastic fluid with  $n = 0.6$  at critical conditions

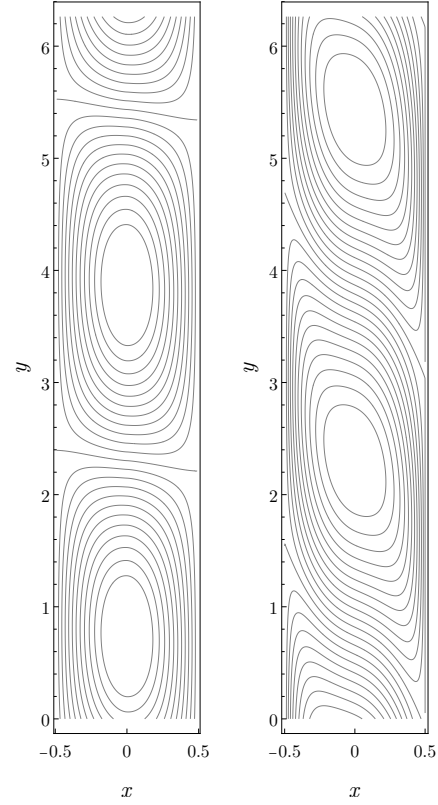


Fig. 9. Dimensionless pressure (left) and temperature (right) contour plot for the perturbations in a dilatant fluid with  $n = 1.4$  at critical conditions

with the smaller  $n$  attains the instability for a lower value of  $R_c$ . Similarly, in Figures 6 and 7 the neutral stability curves of two dilatant fluids are plotted, for  $n = 1.1$  and  $n = 1.4$ , respectively. Again, the higher the  $n$  index, the bigger the value of  $R_c$  that yields the transition to instability.

In order to achieve a deeper knowledge of the flow pattern for the different cases analysed, in Figure 8 and 9 the contour plots of  $P$  and  $\Theta$  are given for a pseudoplastic fluid with  $n = 0.6$  and a dilatant fluid with  $n = 1.4$ , respectively. On the other hand, Figure 10 refers to the limiting case of a Newtonian fluid. By looking at these figures, the shape of the convective cells and their space distribution along the slab can be obtained, thus allowing a better understanding of the effect of the specific rheology for the power-law fluid under exam. In detail, when the fluid is pseudoplastic, one can see a stretched trend of the isobaric lines close to the midplane  $x = 0$ . This phenomenon, which becomes more evident as  $n$  gets smaller, is due to the singularity at the midplane already highlighted in Figure 2. Indeed, in the limit  $x \rightarrow 0$  the function  $F(x)$  vanishes and, thus, according to Eqn. (20)

the second-order derivative  $f''$  disappears from the eigenvalue problem.

Table 1 reports the critical values of  $R$  and  $\alpha$  for decreasing values of  $\delta$ , down to  $\delta = 10^{-40}$ , for two pseudoplastic fluids with  $n = 0.6$  and  $n = 0.7$ , respectively. Similarly, Table 2 reports the critical values of  $R$  and  $\alpha$  for the same decreasing values of  $\delta$ , for two pseudoplastic fluids with  $n = 0.8$  and  $n = 0.9$ , respectively. On the other hand, Table 3 and Table 4 report the critical values for dilatant fluids having  $n = 1.1, 1.2$  and  $n = 1.3, 1.4$ , respectively. The obtained critical values of  $\omega$  turn out to be close to 0, always smaller than  $10^{-4}$  and with an irregular dependence on the input data for any considered case, thus suggesting that  $\omega_c$  is effectively zero. Therefore, the values of  $\omega_c$  are not reported. As can be inferred from the Tables, the critical values  $R_c$  and  $\alpha_c$  are characterised by at least 5 stable significant figures for  $\delta \leq 10^{-20}$ , *i.e.*, they undergo very small changes (practically negligible) when smaller values of  $\delta$  are considered. Moreover, the maximum absolute values of the relative difference in the values of  $R_c$  and  $\alpha_c$  obtained for  $\delta = 10^{-1}$

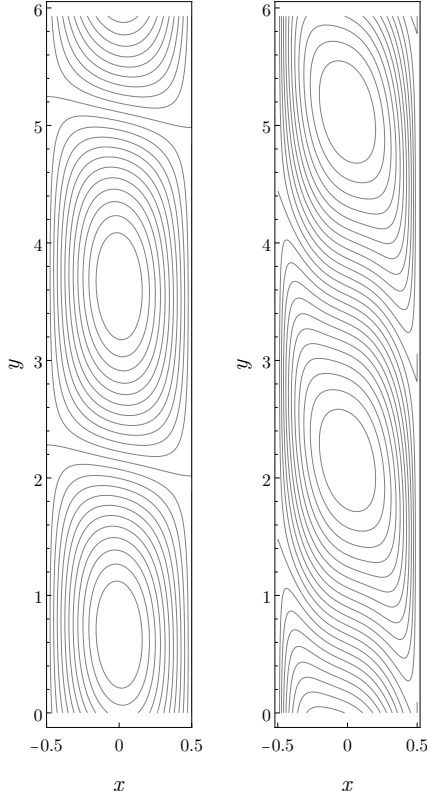


Fig. 10. Dimensionless pressure (left) and temperature (right) contour plot for the perturbations in a Newtonian fluid ( $n = 1$ ) at critical conditions

and  $\delta = 10^{-40}$ , respectively, are 5.8% and 2.9%, which proves a very good convergence of the numerical method adopted.

For both pseudoplastic and dilatant fluids, the results show that the onset of convective instability is obtained for values of  $R_c$  that increase with  $n$ . Relatively low values of  $R_c$  can lead to instability for pseudoplastic fluids, whereas much higher values of  $R_c$  are needed for dilatant fluids. Moreover, the vanishingly small value of  $\omega_c$  in all the considered cases suggests that the convective rolls are stationary.

The obtained pairs of values  $(n, R_c)$  allow one to obtain an interpolation curve, as plotted with a dotted line in Figure 11. The interpolating function has the following fifth-order polynomial expression

$$R_c(n) = 2298.5n^5 - 8616.1n^4 + 13767n^3 - 10963n^2 + 4388.5n - 677.22, \quad (26)$$

for  $0.6 \leq n \leq 1.4$ ,

which leads to values of  $R_c$  very close to those obtained

Table 1. Critical values  $(\alpha_c, R_c)$  for two pseudoplastic fluids having  $n = 0.6$  and  $n = 0.7$ , and sensitivity of results to  $\delta$

$\delta$	$n = 0.6$		$n = 0.7$	
	$\alpha_c$	$R_c$	$\alpha_c$	$R_c$
$10^{-1}$	1.1287	42.273	1.1149	60.899
$10^{-2}$	1.1118	43.402	1.1060	61.713
$10^{-3}$	1.1058	43.942	1.1036	61.990
$10^{-6}$	1.0996	44.606	1.1023	62.182
$10^{-10}$	1.0975	44.831	1.1022	62.208
$10^{-20}$	1.0970	44.890	1.1022	62.210
$10^{-30}$	1.0970	44.891	1.1022	62.210
$10^{-40}$	1.0970	44.891	1.1022	62.210

Table 2. Critical values  $(\alpha_c, R_c)$  for two pseudoplastic fluids having  $n = 0.8$  and  $n = 0.9$ , and sensitivity of results to  $\delta$

$\delta$	$n = 0.8$		$n = 0.9$	
	$\alpha_c$	$R_c$	$\alpha_c$	$R_c$
$10^{-1}$	1.0971	89.090	1.0782	131.912
$10^{-2}$	1.0924	89.708	1.0762	132.315
$10^{-3}$	1.0912	89.885	1.0756	132.432
$10^{-6}$	1.0907	89.964	1.0754	132.479
$10^{-10}$	1.0907	89.968	1.0754	132.481
$10^{-20}$	1.0907	89.968	1.0754	132.481
$10^{-30}$	1.0907	89.968	1.0754	132.481
$10^{-40}$	1.0907	89.968	1.0754	132.481

numerically, the maximum relative discrepancy being lower than 0.6%. The correlation given by Eqn. (26) can be adopted with a good accuracy to determine the critical values  $R_c$  that leads to linear instability for power-law fluids characterised by values of the index  $n$  not present in above Tables and within the range  $0.6 \leq n \leq 1.4$ .

Finally, Figure 12 reports the obtained values  $(n, \alpha_c)$  and their interpolating curve. The Figure shows that, in the considered range  $0.6 \leq n \leq 1.4$ , the critical wave

Table 3. Critical values ( $\alpha_c$ ,  $R_c$ ) for two dilatant fluids having  $n = 1.1$  and  $n = 1.2$ , and sensitivity of results to  $\delta$

$\delta$	$n = 1.1$		$n = 1.2$	
	$\alpha_c$	$R_c$	$\alpha_c$	$R_c$
$10^{-1}$	1.0417	296.444	1.0249	448.233
$10^{-2}$	1.0432	295.612	1.0277	445.757
$10^{-3}$	1.0438	295.320	1.0288	444.814
$10^{-6}$	1.0441	295.170	1.0294	444.263
$10^{-10}$	1.0441	295.163	1.0295	444.231
$10^{-20}$	1.0441	295.163	1.0295	444.230
$10^{-30}$	1.0441	295.163	1.0295	444.230
$10^{-40}$	1.0441	295.163	1.0295	444.230

Table 4. Critical values ( $\alpha_c$ ,  $R_c$ ) for two dilatant fluids having  $n = 1.3$  and  $n = 1.4$ , and sensitivity of results to  $\delta$

$\delta$	$n = 1.3$		$n = 1.4$	
	$\alpha_c$	$R_c$	$\alpha_c$	$R_c$
$10^{-1}$	1.0094	680.550	0.9949	1036.774
$10^{-2}$	1.0132	674.997	0.9995	1025.670
$10^{-3}$	1.0147	672.720	1.0015	1020.826
$10^{-6}$	1.0158	671.239	1.0030	1017.366
$10^{-10}$	1.0158	671.131	1.0031	1017.057
$10^{-20}$	1.0158	671.128	1.0031	1017.046
$10^{-30}$	1.0158	671.128	1.0031	1017.046
$10^{-40}$	1.0158	671.128	1.0031	1017.046

number  $\alpha_c$  is not a monotonic function of  $n$ , though it undergoes only small changes with the maximum relative difference around 9%.

## 5 CONCLUSIONS

The buoyant flow of a power-law fluid saturating a vertical porous slab has been studied. The Ostwald-de Waele rheological model implemented via the power-law

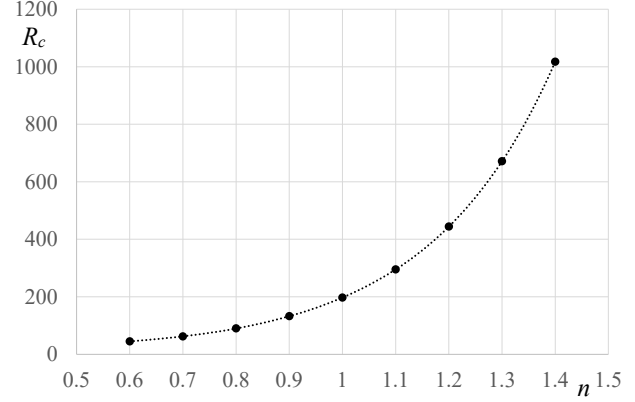


Fig. 11. Interpolation curve of the critical values  $R_c$  as a function of  $n$

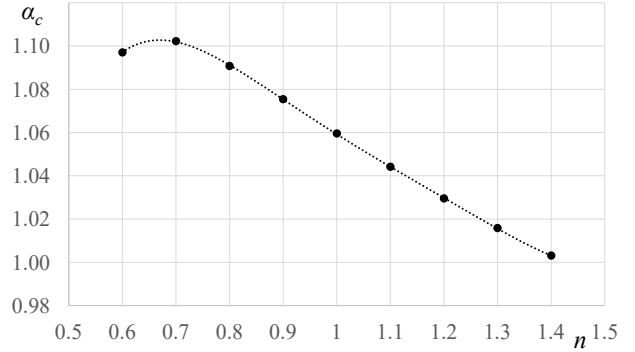


Fig. 12. Interpolation curve of the critical values  $\alpha_c$  as a function of  $n$

extended form of Darcy's law has been adopted to model the seepage flow of both shear-thinning (pseudoplastic) and shear-thickening (dilatant) fluids. Dirichlet's boundary conditions for pressure and temperature have been considered, namely the slab is assumed to be confined by two fluid reservoirs kept at different but uniform temperatures. First, the local mass, momentum and energy balance equations have been written in a dimensionless form and solved to determine the stationary fully developed basic flow. Then, this basic flow has been perturbed through small-amplitude disturbances having the form of normal modes. The resulting dimensionless governing ODEs yield an eigenvalue problem that has been solved numerically for different values of the power-law index  $n$ . The technique employed to find the numerical solution is a shooting method based on a Runge-Kutta solver for initial value problems. In order to manage the singular behavior of the power-law rheology at zero seepage velocity, a smoothing parameter  $\delta$  has been introduced and the results have been traced in the limit  $\delta \rightarrow 0$ . The most

significant conclusions are the following:

- A linear instability arises for every power-law index  $n$  considered, either smaller or larger than unity;
- The transverse modes are the most unstable for both pseudoplastic and dilatant fluids;
- Pseudoplastic fluids turned out to be more unstable than dilatant fluids, as the critical Rayleigh number is an increasing function of  $n$ ;
- The obtained numerical data suggest that the critical angular frequency be zero in any considered case, so that convective rolls are stationary;
- The critical wave number is a non-monotonic function of  $n$ ;
- An accurate fifth-order polynomial expression that interpolates the obtained critical values of  $R$  is provided yielding the linear instability threshold for power-law fluids characterised by values of  $n$  in the range  $0.6 \leq n \leq 1.4$ .

Although the study reported in this paper deals with the linear stability analysis of the basic parallel flow, the time growth of the convection cell amplitude becomes nonlinear after the initiation of the instability. Our results are relevant to the prediction of the parametric conditions leading to the formation of convection cell patterns in the porous layer. However, the time growth of the velocity and temperature amplitude at supercritical conditions shows up its nonlinear nature in the long time. The most important phenomenon is the nonlinear saturation of the growth processes, meaning that the initially exponential growth predicted by the linear theory at late times changes into a slower growth process with a possible asymptotic stationary regime of convection. An example of such an asymptotic behaviour due to nonlinearity is discussed in Barletta [21] with reference to a Newtonian fluid. However, the main practical focus of a weakly nonlinear or fully nonlinear study of the convection regime is on the evaluation of the heat transfer rate across the porous slab when the stationary cellular flow is achieved via the above mentioned nonlinear saturation. Another important aspect is the possible existence of a subcritical instability, namely the onset of convection induced by finite amplitude perturbations. Subcritical instability may happen under parametric conditions incompatible with the onset of a linear instability, viz. a Rayleigh number smaller than its critical value. The existence of such a phenomenon can hardly be detected in a framework based on the linearised governing equations.

As for the heat transfer performance in supercritical conditions, we expect that the thermal energy transport in the supercritical regime is enhanced, compared to the conduction regime obtained for the basic state, by the hori-

zontal flow component due to the formation of convective cells. The rheology of the specific non-Newtonian fluid considered might heavily affect the heat transfer rate in the convective regime. It is reasonable to foresee that the thermal energy transport is a decreasing function of the power-law index  $n$ . In fact, the effective viscosity of the fluid is an increasing function of  $n$  and, thus, for given boundary conditions, the flow rate in the convective cells is expected to be higher for pseudoplastic fluids compared to Newtonian fluids and to dilatant fluids.

All these aspects are challenges for future developments of the analysis presented in this paper.

## ACKNOWLEDGEMENTS

The authors acknowledge financial support from Grant No. PRIN 2017F7KZWS provided by the Italian Ministero dell'Istruzione, dell'Università e della Ricerca.

## REFERENCES

- [1] Bird, R. B., Stewart, W. E., and Lightfoot, E. N., 2002, *Transport Phenomena* Wiley.
- [2] Braun, D. B., and Rosen, M. R., 1999, *Rheology Modifiers Handbook* Elsevier.
- [3] Hoyt, J. W., 1999, *Some Applications of Non-Newtonian Fluid Flow* Elsevier.
- [4] Christopher, R. H., and Middleman, S., 1965, "Power-law flow through a packed tube," *Industrial & Engineering Chemistry Fundamentals*, **4**, pp. 422–426.
- [5] Nakayama, A., and Shenoy, A. V., 1993, "Combined forced and free convection heat transfer in power-law fluid-saturated porous media," *Applied Scientific Research*, **50**, pp. 83–95.
- [6] Shenoy, A. V., 1993, "Darcy-Forchheimer natural, forced and mixed convection heat transfer in non-newtonian power-law fluid-saturated porous media," *Transport in Porous Media*, **11**, pp. 219–241.
- [7] Longo, S., Di Federico, V., Chiapponi, L., and Archetti, R., 2013, "Experimental verification of power-law non-Newtonian axisymmetric porous gravity currents," *Journal of Fluid Mechanics*, **731**, p. R2 [12 pages].
- [8] Tang, G. H., and Lu, Y. B., 2014, "A resistance model for Newtonian and power-law non-Newtonian fluid transport in porous media," *Transport in Porous Media*, **104**, pp. 435–449.
- [9] Gill, A. E., 1969, "A proof that convection in a porous vertical slab is stable," *Journal of Fluid Mechanics*, **35**, pp. 545–547.

- [10] Rees, D. A. S., 1988, “The stability of Prandtl-Darcy convection in a vertical porous layer,” *International Journal of Heat and Mass Transfer*, **31**, pp. 1529–1534.
- [11] Straughan, B., 1988, “A nonlinear analysis of convection in a porous vertical slab,” *Geophysical & Astrophysical Fluid Dynamics*, **42**, pp. 269–275.
- [12] Lewis, S., Bassom, A. P., and Rees, D. A. S., 1995, “The stability of vertical thermal boundary-layer flow in a porous medium,” *European Journal of Mechanics B Fluids*, **14**, pp. 395–407.
- [13] Rees, D. A. S., 2011, “The effect of local thermal nonequilibrium on the stability of convection in a vertical porous channel,” *Transport in Porous Media*, **87**, pp. 459–464.
- [14] Scott, N. L., and Straughan, B., 2013, “A nonlinear stability analysis of convection in a porous vertical channel including local thermal nonequilibrium,” *Journal of Mathematical Fluid Mechanics*, **15**, pp. 171–178.
- [15] Barletta, A., and de B. Alves, L. S., 2014, “On Gill’s stability problem for non-Newtonian Darcy’s flow,” *International Journal of Heat and Mass Transfer*, **79**, pp. 759–768.
- [16] Shankar, B. M., and Shivakumara, I. S., 2017, “On the stability of natural convection in a porous vertical slab saturated with an Oldroyd-B fluid,” *Theoretical and Computational Fluid Dynamics*, **31**, pp. 221–231.
- [17] Lazzari, S., Celli, M., and Barletta, A., 2021, “Stability of a buoyant Oldroyd-B flow saturating a vertical porous layer with open boundaries,” *Fluids*, **6**, p. 375 [9 pages].
- [18] Kefayati, GH. R., 2019, “Lattice Boltzmann method for natural convection of a Bingham fluid in a porous cavity,” *Physica A: Statistical Mechanics and Its Applications*, **521**, pp. 146–172.
- [19] Rees, D. A. S., 2020, “Darcy-Bénard-Bingham convection,” *Physics of Fluids*, **32**, p. 084107.
- [20] Rees, D. A. S., 2022, “Free convection of a Bingham fluid in a differentially-heated porous cavity: The effect of a square grid microstructure,” *Physics*, **4**, pp. 202–216.
- [21] Barletta, A., 2015, “A proof that convection in a porous vertical slab may be unstable,” *Journal of Fluid Mechanics*, **770**, pp. 273–288.